Nuclear Materials and Energy 35 (2023) 101451

Contents lists available at ScienceDirect

Nuclear Materials and Energy

journal homepage: www.elsevier.com/locate/nme

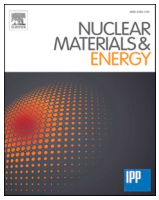

Evolution of the EUROFER97 microstructure during thermal treatment up to 122,000 h

M. Klimenkov *, U. Jäntsch, M. Rieth, A. Möslang

Karlsruhe Institute of Technology (KIT), Institute for Applied Materials - Applied Materials Physics (IAM-AWP), Hermann-von-Helmholtz-Platz 1, 76344 Eggenstein-Leopoldshafen, Germany

ARTICLE INFO

Keywords:
EUROFER97
Long term annealing
Phase transformation
TEM
Laves phase
Z-phase

ABSTRACT

Detailed knowledge of the microstructural evolution of reduce activation ferritic-martensitic steel EUROFER97 after exposure at high temperatures is essential for determining its applications potential. For this proposal, EUROFER97 was annealed in the temperature range between 450 °C and 650 °C for up to 122,000 h (≈14 years) and subsequently analyzed using transmission electron microscopy (TEM) including high resolution TEM and two-dimensional energy dispersive X-ray (EDX) mapping. The study demonstrates the effects of thermal treatment on the size and composition of the precipitates and allows conclusions about their stability. Application of the extraction replication technique was used to analyze composition and morphology of four particle types present in the untreated EUROFER97: $M_{23}C_6$, VN, TaC and TiN with sufficient statistics. The rapid coarsening of the $M_{23}C_6$ precipitates was observed at 650 °C, while the MX particles were found to be more stable upon thermal treatment. It has been proved that new Laves (WFe_2) and modified Z-phases (Cr(V,Ta)N) precipitates are formed in the temperature range from 500 °C to 600 °C. The detailed analysis allows the drawing a time–temperature formation diagram for these two phases, which could be valid for alloys with composition similar to EUROFER97.

1. Introduction

EUROFER97 – the European reduced activation feritic-martensitic (RAFM) reference material with 9Cr1.1 W0.2 V0.14Ta0.42Mn and Fe bal. is considered as a primary candidate for application at the first wall components of ITER and DEMO respectively [1,2]. The plasma facing components are supposed to be subjected to complex thermomechanical stresses and high irradiation doses. Knowledge of the microstructural stability during long-term thermal treatment is an important requirement for a sufficiently reliable prediction of the service life. One of the key factors affecting the mechanical properties of steels is the presence and spatial distribution of secondary phase particles, which precipitation during tempering closely related to the formation of the steel microstructure. In practice, microstructure is controlled by changing the concentration of minor alloying elements and heat treatment conditions, including the hardening process [3,4].

The chemical composition of EUROFER97 was selected based on activation calculations of composition isotopes and experience with RAFM precursor alloys of the OPTIFER type [4]. The main objective was to replace the elements with long decay periods such as Ni, Mo and Nb by W, V and Ta. TEM characterization of the microstructure of EUROFER97 has already been reported in several publications. Information on the size, number density and spatial distribution of precipitates is important to understand the influence of alloying elements on the microstructure and thus on the mechanical properties in general, allowing further optimization of the chemical composition of RAFM steels [5–8]. The $M_{23}C_6$- and Ti, V- or Ta-rich MX-type precipitates were found and analysed in TEM and SEM [7,8]. W is mainly added as a solution strengthening element but can also be present in $M_{23}C_6$ precipitates. Ta has a strong affinity for C, and thus it can be expected that Ta is largely used for the formation of TaC precipitates. TaC and TiN contribute to grain size stabilization by suppressing the growth of primary austenite grains at temperatures higher than the $\alpha \rightarrow \gamma$ transition. It was also shown that the addition of Ta leads to grain refinement in F82H alloy [9]. Small amounts of V are added to improve creep strength and impact behaviour [10]. VN particles form at temperatures below the $\alpha \rightarrow \gamma$ transition and thus influence the formation and stabilization of laths. The precipitation of $M_{23}C_6$ carbides on the grain and lath boundaries at 500°-600 °C additionally stabilizes the structure.

The thermally induced alteration of the microstructure of ferritic-

* Corresponding author.
E-mail address: michael.klimenkov@kit.edu (M. Klimenkov).

https://doi.org/10.1016/j.nme.2023.101451
Received 24 February 2023; Received in revised form 12 May 2023; Accepted 17 May 2023
Available online 22 May 2023

martensitic steels is a complex process involving the dissolution or coarsening of existing precipitates, precipitation from the solid solution, and the formation of new phases, such as Laves- and modified Z-phase. This process consequently leads to a coarsening of the laths and the grains and finally to a degradation of the mechanical properties and softening of the material. However, the processes occur differently at each temperature, and knowledge of them is essential for the application of EUROFER97 as a structural material.

The microstructural stability of recently developed RAFM steels, which include EUROFER97, F82H and CLAM steels, has been reported in several publication [11–16]. Pronounced coarsening of existing precipitates and grains in RAFM steels was observed at 650 °C and higher temperatures, implying increased diffusion and segregation of alloying elements [14]. The formation of Z-phase in RAFM steels has been reported only for irradiated materials, for which irradiation accelerates diffusion and thus its formation [17]. It is suggested that the formation of Z-phase leads to a decrease in creep strength, as the phase forms at the expense of highly dispersed VN particles, which have a more significant effect on the stabilization of the microstructure than micrometer-sized Z-phase particles. The thermally induced formation of the Z-phase at 550C° has been reported for V-containing steels with 9–12 % Cr, that do not belong to the RAFM steel class [18–20]. However, it can be assumed that the Laves phase forms in RAFM steels under similar conditions.

The formation of Laves phase particles in RAFM steels takes place in the range from 550 °C to 650 °C [11,13,15,16]. A study with an annealing time of up to 100 k hours on the alloy F82H shows the formation of the Laves phase in the temperature range from 550 °C to 650 °C [16]. The steel was analyzed by XDR analysis on the replica, which provides information on the occurrence of different phases but not on the size of the precipitates. The formation of Laves phase at 550 °C was reported for CLAM steel [21]. It is widely believed that the formation of the Laves phase reduces the thermal stability of the microstructure at high temperatures and adversely affects the mechanical properties of the steel [15,16]. The formation mechanism of the Laves phase in the RAFM steels is not clear, since it is not precisely known whether the Laves phase is formed from the W contained in the $M_{23}C_6$ precipitates or from the W in the solid solution. However, it is known that the formation of the Laves phase leads to a degradation in strength and ductility.

The objective of the present work is to demonstrate the temperature effect on the size and distribution of precipitates in EUROFER97 during long-term aging in the range from 450 °C to 650 °C for up to 122,000 h and to determine the conditions for nucleation and coarsening of the Laves and Z-phases and to determine the conditions for nucleation and coarsening of the Laves and Z-phases. The results obtained are important for understanding the microstructure evolution and assessing the limits of the practical application of EUROFER97 at high temperatures.

2. Materials and methods

2.1. Thermal treatment and TEM examination

All samples examined in this work were taken from creep specimens prepared from the first batch of EUROFER97 [3]. The used semi-finished product was a forged round bar (heat E83699) with a diameter of 100 mm in the condition as delivered from the manufacturer (Saarschmiede, Germany), i.e., after a heat treatment of 980 °C/30′ air cooling + 740 °C/90′/ air cooling. The creep specimens were produced parallel to the rod axis with screw heads of 5 mm and 8 mm in diameter. The creep tests were performed in electrical furnaces with three vertical heating zones in normal atmosphere (i.e., in air). The test temperatures were controlled with three PtRh-Pt thermocouples and kept constant at ± 2 K by means of three PID control units.

For TEM sample preparation, we used only the screw heads of the creep specimens. This ensured that only undeformed (stress-free) material was analysed in the present work. This enables us to study only aging effects on microstructure and not an additional mixture of deformation effects and resulting artifacts. In the following, we denote the creep conditions of the screw heads as annealing time and annealing temperature.

The annealing conditions (e.g. temperature and annealing time) of samples chosen for TEM examination are given in Table 1. This list includes samples with the highest annealing time for each temperature and samples with lower annealing times to show microstructure evolution. The highest annealing time varied from 17kh for 650 °C to 122kh for 550 °C. To improve the readability of the manuscript, treatment times are rounded to the nearest thousand hours (kh). The samples for TEM analysis were obtained from the undeformed parts of the tensile specimens to study the pure temperature effect and avoiding the complex influence of deformation on the microstructure.

The microstructures of the specimens have been characterized on thin foils prepared by standard electrochemical etching [7] and carbon extraction replicas [6,22] using transmission electron microscope Talos F200X equipped with four energy-dispersive X-ray (EDX) detectors for two dimensional elemental mapping. The resolution of the EDX detector is ≤ 136 eV at Mn-Kα, as specified by the manufacturer. The spot size of about 1.0–1.2 nm with a step size of 1 nm was used to generate high-resolution elemental analyses. For the overview maps, the spot size ranged from 2 to 5 nm with a step size of 10 nm.

2.2. Microstructure of as-delivered EUROFER97

The microstructural changes of EUROFER97 caused by the thermal treatment were determined by comparison with the microstructure in the as-received state after the standard treatment procedure (980 °C/30′ air cooling + 740 °C/90′/ air cooling) [23]. The material has a martensitic lath structure with average lath thickness of 250 nm and grains of several tens microns. Identification and spatial distribution of second phase precipitates in EUROFER97 was reported in ref. [7], applying the 2D EDX mapping in combination with HRTEM imaging. In total four different types of precipitates have been detected: $M_{23}C_6$, TaC, VN and TiN. The study was performed on thin foils where the precipitates are embedded in the matrix [7]. Since the experiments in the present work were performed using carbon replicates, the untreated material was also analyzed using carbon replica to provide a reliable comparison. In addition, the replica provides more reliable analysis of the precipitates composition.

Fig. 1 shows a typical precipitate replica prepared from as-delivered EUROFER97. The distribution of Cr (green) reflects position of $M_{23}C_6$ precipitates (Fig. 1a), V (blue) positions of VN, Ta (red) positions of TaC and Ti (yellow) positions of TiN particles (Fig. 1b). It was also found that TiN precipitates are frequently surrounded by VN or/and TaC phases, which could be a reason for some V and Ta content inside TiN particles (Fig. 1b). Their chemical composition and average size are given Table 2. Since the carbon film used for replication does not allow reliable detection or quantification of carbon in carbides, these and nitrogen content were not analysed. So only the metals present in the precipitates were included in the data table. It has been shown that identification of precipitates by their metal content is much more meaningful than measuring carbon or nitrogen. For this proposal, the main composition element can be used for fast and reliable identification of precipitates in

Table 1
Thermal treatment conditions of the samples selected for TEM examination.

Annealing temperature (°C)	Annealing time (h)				
450	18,596	**31,801**			
500	32,283	**108,509**			
550	20,585	38,730	74,917	110,881	**121,560**
600	1047	9971	21,339	**35,688**	
650	5787	11,565	**17,006**		

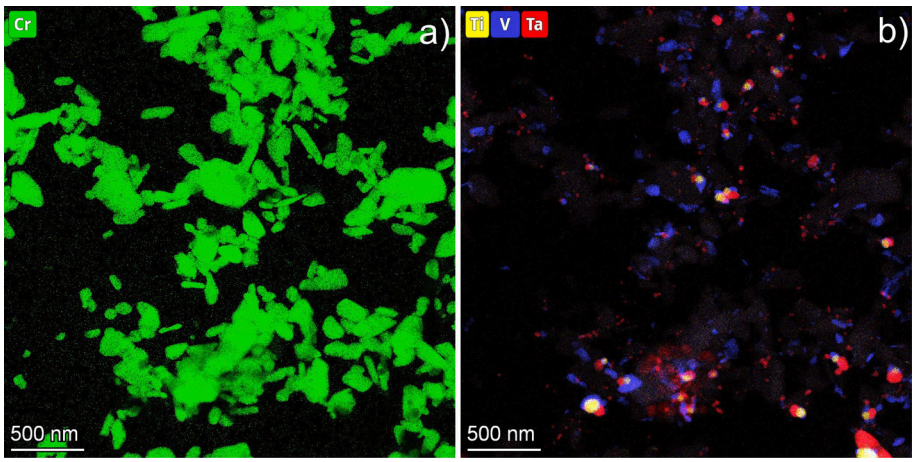

Fig. 1. EDX analysis of precipitates replica from as-delivered EUROFER97. Part (a) shows distribution of $M_{23}C_6$ precipitates and part (b) the distribution of MX (VN, TaC and TiN) precipitates.

Table 2
Composition and average size of precipitates measured on replica in as-delivered state. With yellow color are marked major elements used for their identification in elemental maps. The contents of carbon and nitrogen were omitted.

Type	Composition (weight %)			
	$M_{23}C_6$	VN	TaC	TiN
Cr	64.8 ± 0.8	4.5 ± 0.5	—	—
V	1.0 ± 0.2	81.0 ± 2.5	11.0 ± 1.5	11.4 ± 1.2
Ta	———	14.5 ± 2.0	89.0 ± 1.5	
Ti	———	———	———	88.6 ± 1.2
Fe	26.4 ± 1.1	———	——	–
W	7.8 ± 0.7	———	———	———
Average size (nm)	110 ± 4	48 ± 4	45 ± 2	53 ± 2

element maps (Table 2).

The composition and size of the precipitates measured on the replica largely correspond to the data from ref. [7] measured on the bulk samples. However, the measurement of composition on replica instead of on embedded particles, provides more accurate results.

The number density of precipitates was not calculated, as this information is not available by investigating replica. However, it can be noted that the number of TaC particles normalized to the area studied is approximately equivalent to the number of $M_{23}C_6$ precipitates, while the number of VN particles is 2.5 times larger. The TaC and TiN precipitates were found to be randomly distributed in the specimen, while VN and $M_{23}C_6$ precipitates predominantly decorate the grain or lath boundaries.

2.3. Identification of Laves phase and Z-phases

The analysis of thermally treated material shows the formation of particles composed of two additional phases, which were identified as the Z- and Laves phases. For more comprehensive statistics, it is important to find a reliable identification criterion for these new phases in the elementary maps to avoid time-consuming structural analysis on individual particles. The Z-phase is known as nitride phase with CrXN composition, where X is typically Nb. In the V- and Ta-containing alloys, which include EUROFER97, the modified Z-phase was detected with the Cr(V,Ta)N composition [18]. In the V and Cr maps elemental maps Z-phase particles show a similar contrast to VN or to $M_{23}C_6$ particles. Reliable identification of the Z-phase is only possible if these two these elements are considered. Ta and Fe contents of about 15% can also be considered in the verification. (Table 3). The chemical composition of these phases formed in the 500 °C-600 °C range was measured by EDX analysis on the replica (Table 3, Fig. 2).

The intermetallic Laves phase with WFe_2 composition was detected

Table 3
Chemical composition of Z- and Laves phases measured by EDX methods.

Elements	Composition (weight %)	
	Cr(V,Ta)N (Z-phase)	WFe_2 (Laves phase)
Cr	42.2	13.8
V	45.7	———
W	———	29.4
Fe	4.0	56.8
Ta	8.1	———

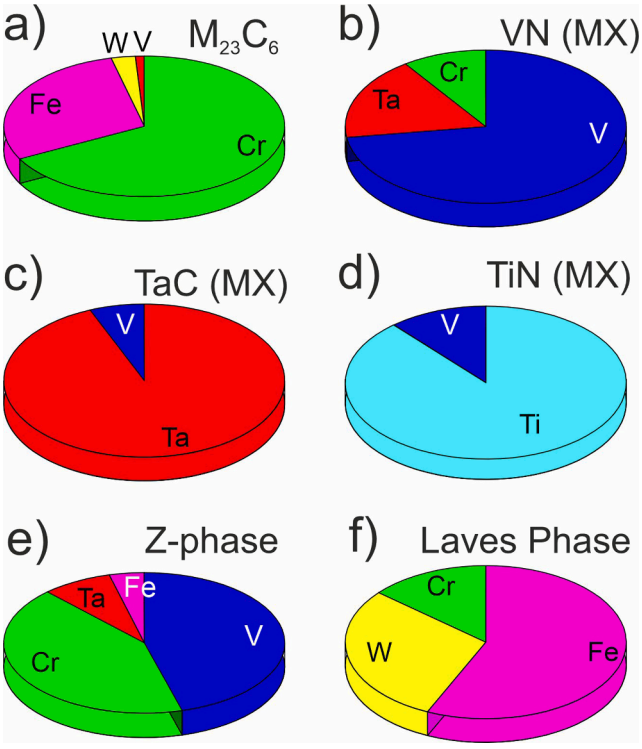

Fig. 2. Chemical composition of the precipitates measured on the replica. The composition includes only the content of metals, while the C and N contents have been omitted (see text for details).

in RAFM steels in which W is used instead of Mo [6]. It is also known that Laves phase is not stable at high temperatures, and it has a long nucleation and growth time [12]. The Laves phase particles can be reliably differentiated from other phases by their comparatively high W content. Additionally, it can be verified by consideration of the Fe content, which together with W accounts for ~ 85% of the total composition of the particles of the Laves phase (Fig. 2).

Fig. 3 shows an example Laves and Z-phases identification in the material annealed at 550 °C for 122 kh. A Z-phase particle with the size of ~ 600 nm is marked with a yellow arrow in the Cr (a), V (b), and N (c) reflecting its CrVN composition. The VN particle on the other hand is visible in sufficient contrast in V (b) and N (c) maps, is invisible in the Cr map (a). In this way, Z-phase particles can be clearly distinguished from VN particles and from $M_{23}C_6$ particles containing Cr but no V. The Z-phase particles have a size of up to 1 μm and are thus in most cases significantly larger than the VN particles, whose maximum size does not exceed 75 nm.

The Laves phase particle of several hundred nm size is marked with a red arrow in W (e) and Fe (f) maps (Fig. 3). The high W content in the WFe_2 phase allows its clear distinction from $M_{23}C_6$ particles. In the combined VW map (d), the Laves phase (yellow) and Z-phase particles (blue) are clearly visible. The maps of Ti (g) and Ta (h) show the distribution of MX precipitates, whereby Z- and Laves phase are invisible in these maps. Additional measurements using EELS method was performed to verify N content in Z-phase.

The correct identification of the new phases in elemental maps was verified by analysing their crystalline structure using high-resolution TEM (Fig. 5 and Fig. 4). The (CrNb)N Z-phase with tetragonal structure was typically found in the Nb containing creep-resistant steels. Increased investigation of V- containing steels (which include the RAFM steels) after long-term creep experiments during last 2 decades shows the formation of modified Z-phase with CrVN composition and cubic (a = 0.413 nm) or tetragonal structure (a = 0.286 nm, c = 0.739 nm) [19]. In Fig. 4 is shown a Z-phase particle that was identified in Cr and V elemental maps. The FFT pattern obtained from a HRTEM image is shown the part (c). The structure identification program clearly proves (Fig. 4d) that the structure of the orientation in the [011] zone axis corresponds to the modified Z-phase with cubic structure (ICSD: 626365) [6]. In the alloys containing V and Ta, the modified Z-phase with Cr(V,Ta)N composition and cubic structure was detected [18,24].

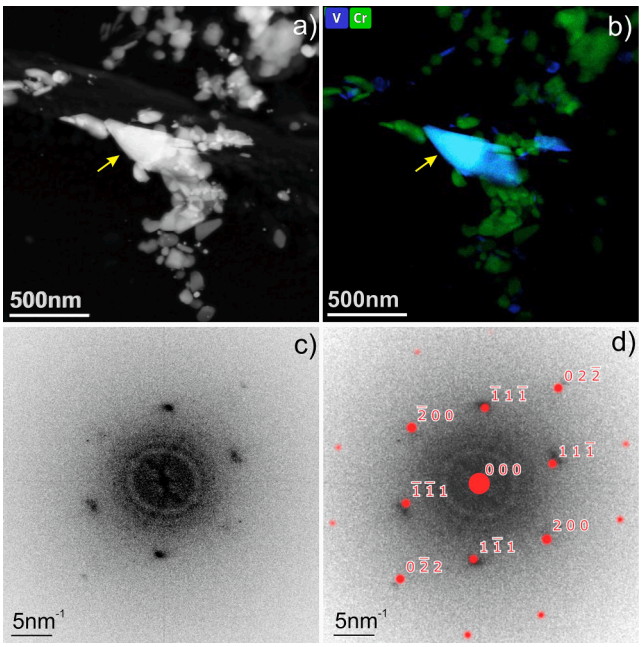

Fig. 4. HRTEM analysis of a Z-phase particle oriented with [011] zone axis. The particle is images with the blue colour in elemental map. HRTEM image (b) was obtained from the area marked by a circle in the part (a). The corresponding FFT pattern shown in (c) was superimposed with simulated diffraction patterns for Z-phase (d).

The intermetallic Laves phase with WFe_2 composition (ICSD: 632621) has a cubic structure [6]. The HRTEM image of crystalline structure shown in Fig. 5b was obtained from a particle marked with red circle in Fig. 5a. The corresponding FFT image (part c) show the presence of stacking faults with random periodicity. However, despite these defects, the position of the diffraction spots could be clearly identified.

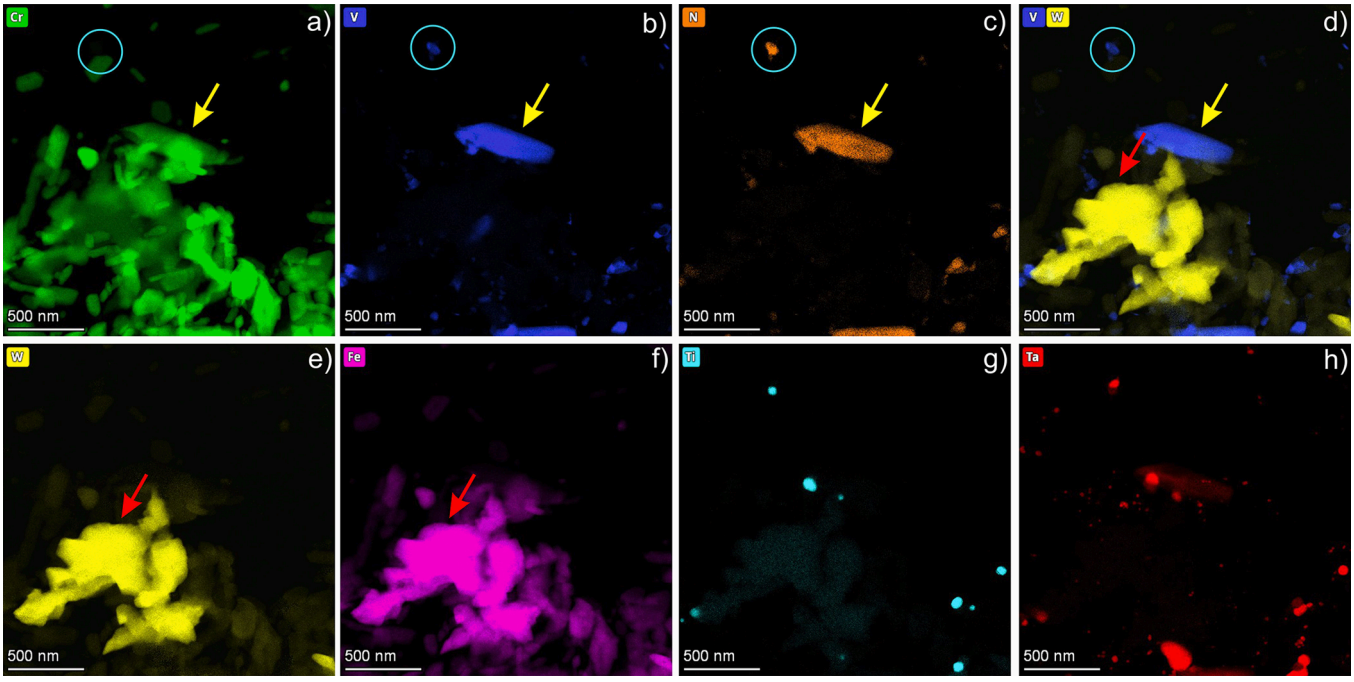

Fig. 3. EDX analysis of precipitates replica from EUROFER97 annealed at 550 °C for 122kh. The corresponding elements are indicated in the maps. For more details, see the text.

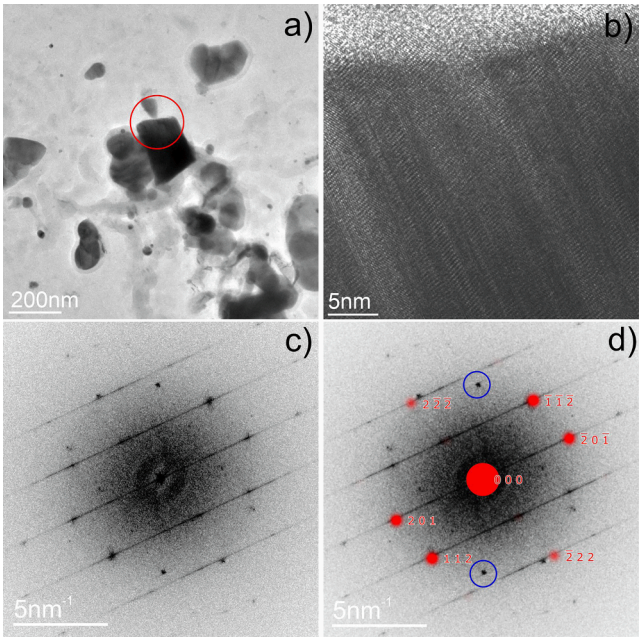

Fig. 5. HRTEM analysis of a Laves phase particle oriented in the [13 $\bar{2}$] zone axis. The HRTEM image (b) was obtained from the area marked by a circle in the part (a). The corresponding FFT pattern shown in (c) was superimposed with simulated diffraction pattern for Laves phase (d).

The structure fitting procedure shows that this particle is oriented with the [13 $\bar{2}$] zone axis to the electron beam. The corresponding simulated diffraction pattern using ICSD data is shown in the overlap of FFT pattern in Fig. 5d. The marked with blue circle diffraction spots originate from the slightly overlapping $M_{23}C_6$ particle that is visible on the upper part of the Laves phase particles. Analysis of the literature demonstrates that the Laves phase of various modifications often forms with stacking faults [25].

In summary, this section shows that the Z-phase and Laves phase particles in EUROFER97 form after long-term treatment and the particles can be identified in elemental maps.

3. Microstructure of annealed samples

3.1. Annealing at 450 °C

The maximal annealing time at 450 °C was 32kh. The TEM examination of material after maximal annealing time show that microstructure of precipitates and texture remained largely stable. No remarkable changes in the morphology of the precipitates were observed and no formation of new phases were detected. The distribution of precipitates is identical to the as-delivered EUROFER97 as it is shown in Fig. 1.

3.2. Annealing at 500 °C

Two samples annealed at 500 °C for 38kh and 109kh were examined by TEM. EDX analysis of the replica shows that there is no remarkable alteration of the size of the existing precipitates even after an annealing time of 109kh (Fig. 6a,a'). The Laves phase particles were detected only in the material after 109kh annealing. Z-phase particles could not be identified at this temperature. In the V/W overview map (Fig. 6a'), the Laves phase particles with the sizes up to 250 nm are well visible with the yellow contrast. The maps obtained with higher magnification show that, in addition to the large particles (red arrow in b,b',c,c'), numerous Laves phase particles with size < 50 nm (white arrows b,b',c, c') have formed. The average size of Laves phase particles was measured as 45 nm.

It is clear that large $M_{23}C_6$ particles (green color) often serve as the nucleation sites for Laves phase particles. The $M_{23}C_6$ phase exhibits an 8% W concentration (Table 1), which facilitates the formation of Laves phase particles. The TaC or VN particles does not contain W in a detectable concentration.

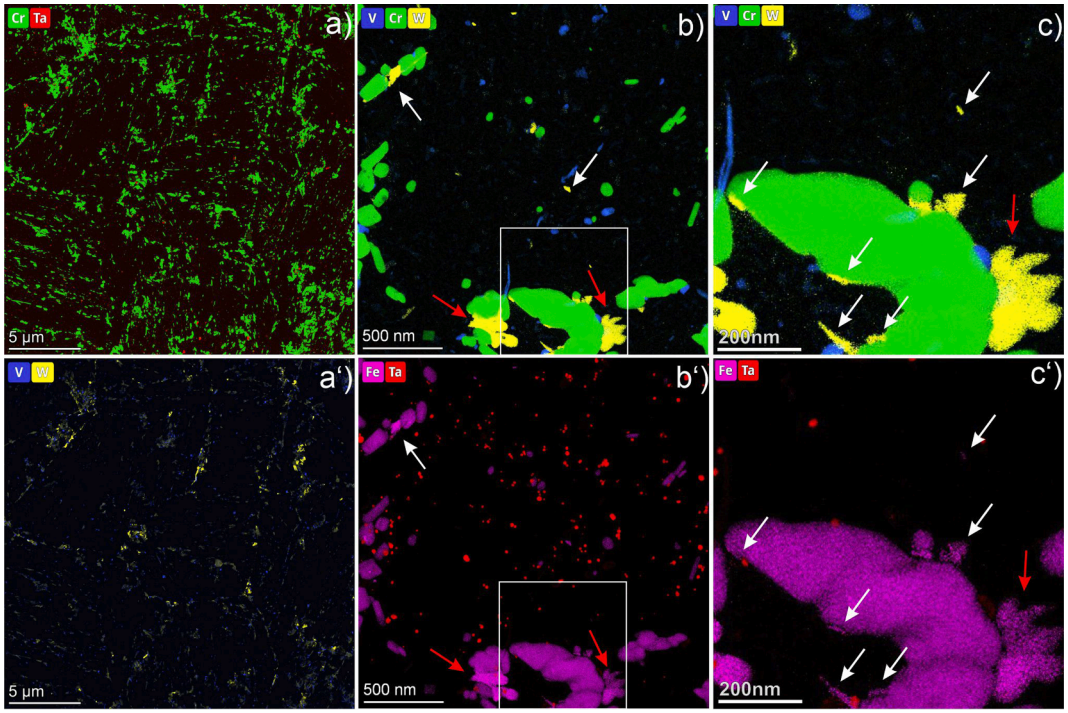

Fig. 6. EDX analysis of precipitates replica from EUROFER97 annealed at 500 °C for 109kh. The designations of the elements for this analysis are shown in the figures. The overview of the precipitates is shown in parts (a,a'), while the distribution of the elements is shown at higher magnification. Parts (c,c') show a magnified section of the images in (b,b').

3.3. Annealing at 550 °C

Microstructure of four samples annealed at 550 °C for 21kh, 38kh, 74kh and 122kh were examined by TEM. The elemental maps shown in Fig. 7 and Fig. 8 demonstrate evolution of precipitates with annealing time. Fig. 7 provides distribution of precipitates on the large scale, while the higher magnification used for the obtaining the maps in Fig. 8 shows the detailed distribution of smaller precipitates. The Laves phase precipitates were identified after already 21kh annealing to be formed at the grain boundaries (yellow particles in Fig. 7a and Fig. 8a). Two of them are also marked with yellow arrow in the Fig. 8a,a'. At the larger annealing time Laves phase particles were also found to form inside grains (yellow particles in Fig. 7b and Fig. 8b). Both, the number and the size of Laves phase particles noticeably increase. After 122kh annealing the size of Laves phase particles that can achieve 1–2 μm.

The formation of the Z-phase was observed at 38kh and higher annealing time. In the sample annealed for 71kh, the particles of the Z-phase can reach a size of several hundred nanometers (blue particle in Fig. 8b). It was found that in addition to the large Z-phase particles of 600–1000 nm, there is a large number of small particles of 30–100 mm were formed (blue spots in Fig. 7c).

In material annealed for 122kh further coarsening and of Z- (blue color) and Laves phase (yellow color) was observed (Fig. 7c,c', Fig. 8c, c'). The frequent close spatial occurrence of these phases may indicate that their formation is interrelated (Fig. 7c). Examination of the $M_{23}C_6$ precipitates shows that their size and distribution do not change remarkably even at the highest annealing time (Fig. 7a,',b',c').

3.4. Annealing at 600 °C

Three samples annealed at 600 °C for 10kh, 21kh and 36kh were available for TEM examination. Investigations demonstrate the formation of Z-phase at all annealing times, whereas the presence of Laves phase does not detected at this temperature. Fig. 9 demonstrates the presence of Z-phase in material after 10kh annealing. The particle is marked with a square in the combined V-Cr-Ta map. The particles of the VN and Z-phases can be identified by the V/Cr ratio. It can be seen that the Z- (turquoise arrow) and the VN-phase (yellow arrow) are attached (Fig. 9). The composition of these particles correlates well to that given in Table 2. It can be assumed that VN particles serve as locations for the formation of the Z-phase. The density of Z-phase particles is notably low. In the material annealed for 36kh, the Z-phase particles could achieve a size of up to ~ 1.5 μm and their number density significantly increases. Also, the measured 180 nm average size of $M_{23}C_6$ particles in material after 36kh annealing indicates notable coarsening process at this temperature.

3.5. Annealing at 650 °C

Three samples annealed at 650 °C for 6kh, 11kh and 17kh were available for TEM examination. Investigations and extensive analysis do not show the formation of new precipitates. The key thermal treatment effect on the microstructure at this temperature is significant growth of the existing precipitates. Fig. 10 illustrates the coarsening of the $M_{23}C_6$ precipitates. the average size increases from 110 nm in the initial state to 320 nm after 17kh treatment, while some particles reach a size of>1 μm. The size of MX precipitates does not changed significantly indication stability of these phase at 650 °C.

4. Discussion

This study involves the detailed microstructural examination of EUROFER97 after annealing in the temperature range from 450 °C to 650 °C for up to 122 k hours. Thermal treatment initiates two different processes that lead to a change in the precipitate structure and consequently have an influence on the mechanical properties. These include the time- and temperature-dependent coarsening or dissolution of existing precipitates as well as changes of their composition and the formation of new precipitates e.g., Laves and Z-phase.

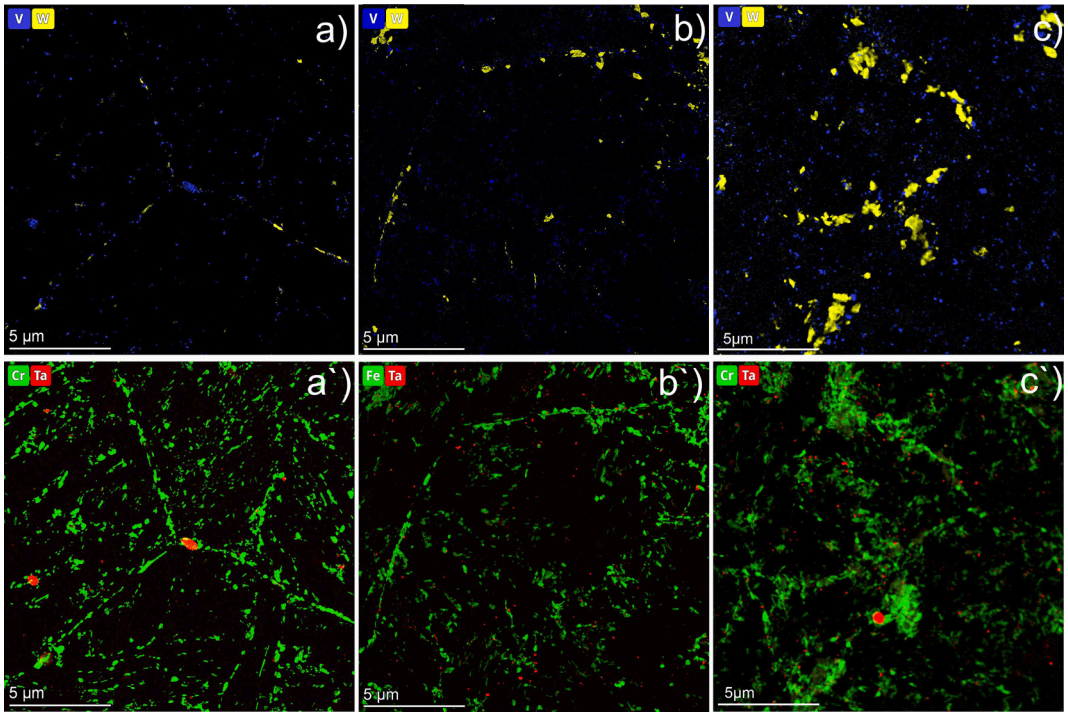

Fig. 7. EDX analysis of precipitates replica from EUROFER97 annealed at 550 °C for 20.7kh (a, a'), 75kh (b, b') and 122kh (c,c'). The corresponding elements are indicated in the maps.

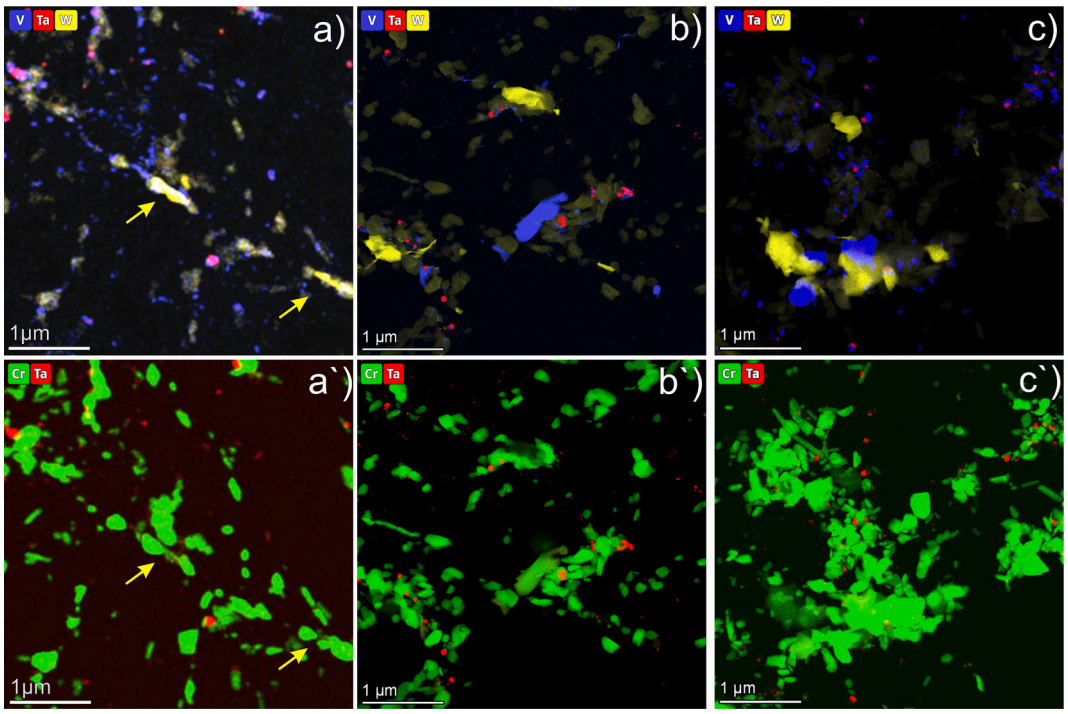

Fig. 8. EDX analysis of precipitates replica from EUROFER97 annealed at 550 °C for 21kh (a, a'), 75kh (b, b') and 122kh (c,c').

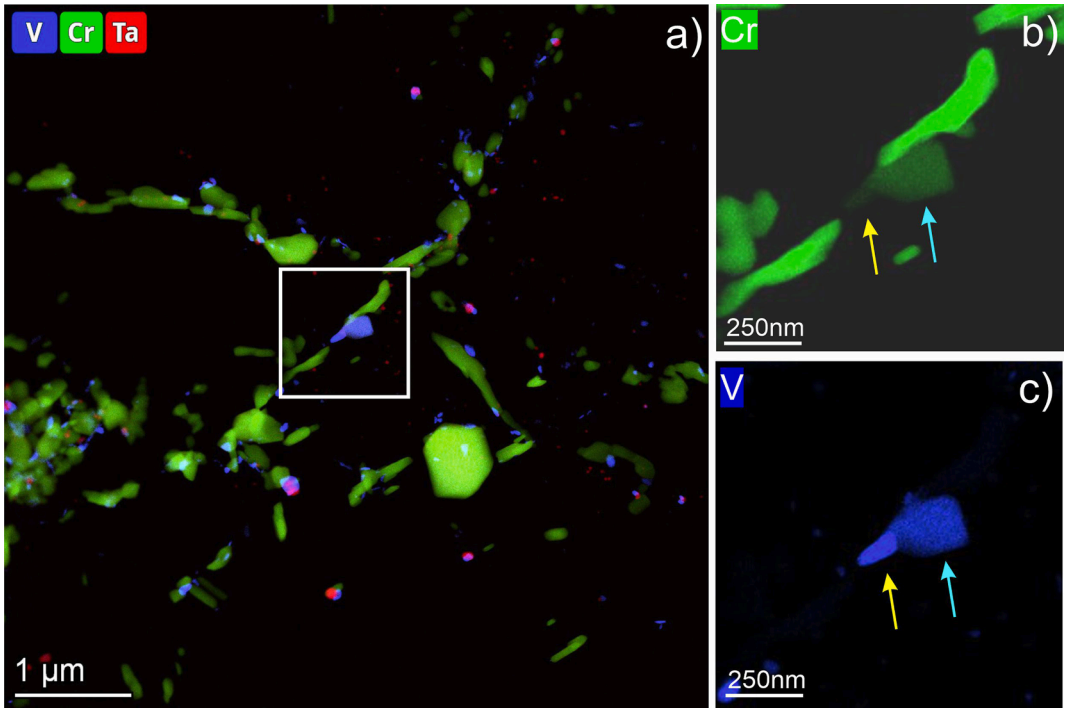

Fig. 9. EDX analysis of precipitates replica from EUROFER97 annealed at 600 °C for 10kh (a). The Cr and V maps are shown in the parts (b) and (c) respectively. The Z-phase particle is marked with turkis arow whereas VN particle is marked by yellow arrow.

4.1. Temperature- and time-dependent alteration of existing precipitates

Thermal annealing leads to a size modification of the precipitates present in EUROFER97. The size increase of $M_{23}C_6$ precipitates was measured at temperatures above 550 °C, while at lower temperature particle size slightly decrease (Fig. 11a). Pronounced coarsening after 17kh annealing was observed at 650 °C (increase in average size by a factor of ~ 3), whereas the growth rate is significantly lower at lower temperatures. At 550 °C, a moderate increase to the size of $M_{23}C_6$ particles was observed, from 110 nm to 155 nm after 122kh with little growth observed up to 20kh. A moderate decrease in the precipitate size was observed at 450 °C and 500 °C (Fig. 11a), that indicates the dissolution process of the $M_{23}C_6$ precipitates during long-term annealing.

The influence of heat treatment on the size of MX precipitates (e.g.

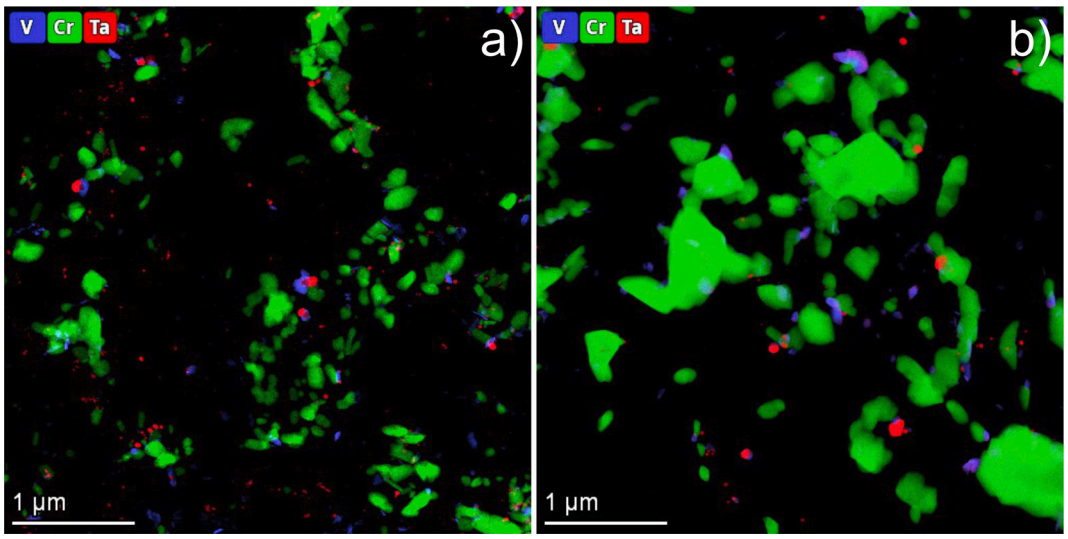

Fig. 10. EDX analysis of precipitates replica from as-delivered EUROFER97 (a) and annealed at 650 °C for 17kh (b). The images demonstrate the coarsening of $M_{23}C_6$ precipitates.

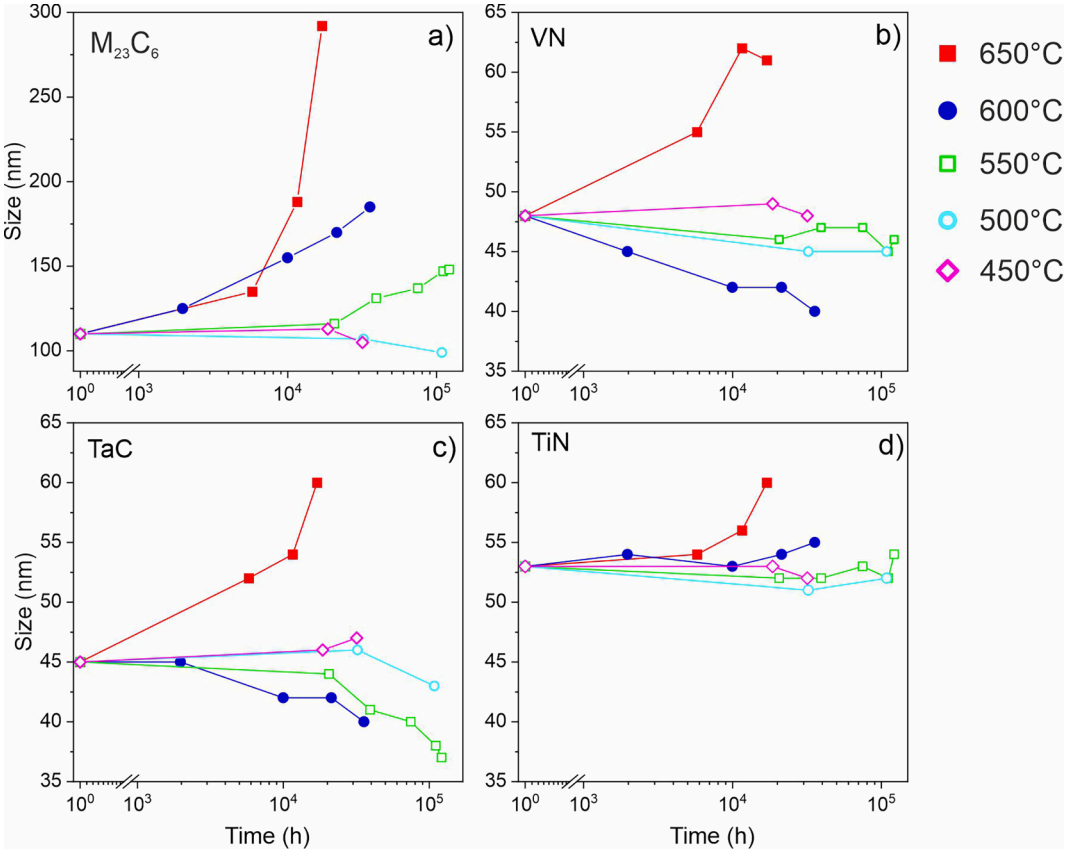

Fig. 11. Size evolution of $M_{23}C_6$ (a), VN (b), TaC (c) and TiN (d) precipitates depending on annealing time and temperature.

VN, TaC and TiN) is less pronounced than on the $M_{23}C_6$ particles. Their size increases for about 20% at 650 °C, whereas at lower temperature it remains almost stable or decreases (Fig. 11b-d). The significant decrease in VN particle size observed at 600 °C is likely due to increased V and N consumption for the formation of the Z-phase. At the lower temperatures where the Z-phase does not form, the VN particles show minor size decrease even at times > 10^5h. The TaC particles also grow at 650 °C, while their size decreases at lower temperatures (Fig. 11c). A particularly pronounced decrease from 45 nm to 36 nm was observed for annealing times > 100kh at 550 °C. TiN particles also grow at 650 °C, but their size remains stable at all other temperatures.

Annealing at 500 °C and higher results in changes of the composition of the precipitates (Fig. 12). For this diagram, the data from the samples with the longest annealing time at each temperature were used. The data from the samples annealed at 450 °C were not taken for this analysis, as the changes of composition were not detected. The $M_{23}C_6$ precipitates indicate an increase in Cr content and a decrease in Fe content with increasing annealing temperature, while the W and V contents do not

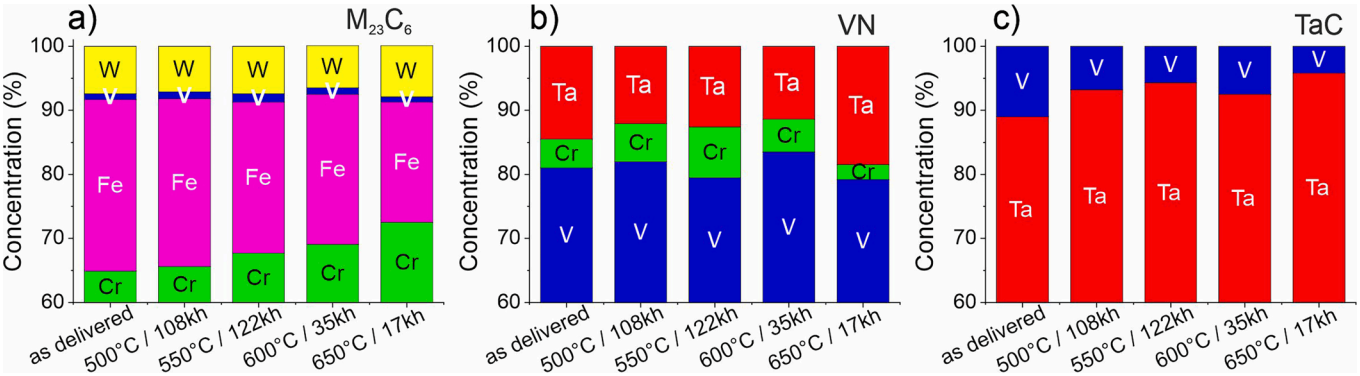

Fig. 12. Evolution of concentrations of metallic components (wt. %) of $M_{23}C_6$ (a), VN (b) and TaC (c) precipitates with annealing under different conditions.

change significantly (Fig. 12a). The composition of the MX precipitates shows only minor changes. The Ta content in the VN particles increases remarkably at 650 °C - the temperature at which coarsening was also observed. At the lower temperatures, the concentration variations are in the range of 5%, which can be considered as an uncertainty range (Fig. 12b). A systematic decrease in V content from 12% to 5% with annealing temperature was observed for TaC particles (Fig. 12c). It is reasonable to assume that this behavior is related to the precipitation of Ta from the solid solution, whose decreasing concentration can lead to loss of ductility.

There are few results reporting compositional modification of precipitates by annealing in similar alloys. Eggeler at all [6] reports microstructural analysis of 12% CrMo steel after long term creep experiment at 550 °C for 139kh. They show that Cr content in $M_{23}C_6$ precipitates increases from 68% to 73%, which is consistent with our results. This effect has been also been reported by Aghajani et al. [26] in 12% Cr (German grade: X20) martensitic steel.

4.2. Formation of Laves- and Z-phase

TEM analyses show that annealing in the range of 500 °C to 600 °C leads to the formation of modified Z-phase and Laves-phase particles, which are not present in the untreated EUROFER97. The V-containing Z-phase has a crystal structure with a smaller lattice constant than the conventional, Nb-containing Z-phase, and as a result it was referred to as modified Z-phase [20]. Their time–temperature formation diagram is shown in Fig. 13. Since the amount of data is limited, the time–temperature conditions for their formation were obtained approximately. The modified Z-phase was found at 600 °C and 550 °C. At 550, it was only observed after annealing times of at least 39kh, whereas at

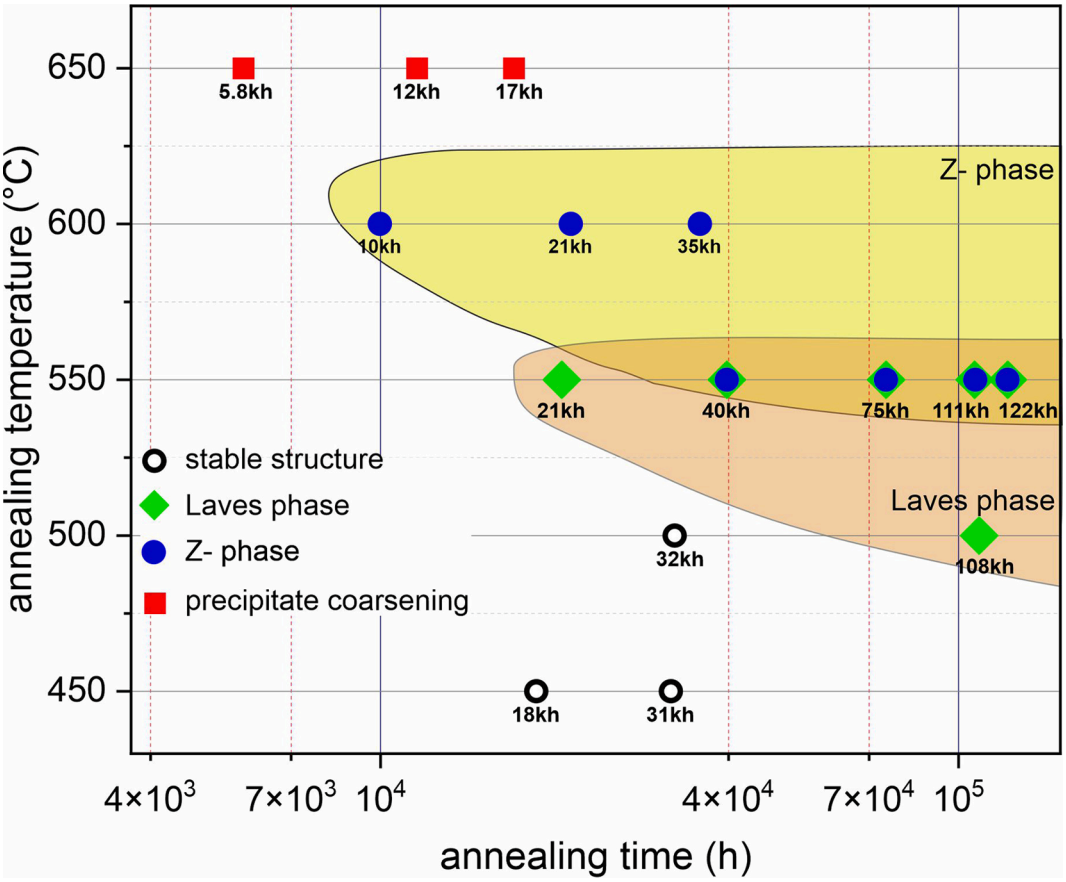

Fig. 13. The time-temperature precipitation diagram shows the conditions for the formation of Laves and Z-phases.

600C, Z-phase was found after all annealing times studied. It can be assumed that its the formation starts at 600 °C after a few thousand hours annealing. At the initial formation stages (600 °C/10kh), the small Z-phase particles were often found in association with VN particles (Fig. 9). This indicates that VN particles serve as nucleation sites for formation of Z-phase. The size and number density of the Z-phase increases rapidly with annealing time, reaching a size of up to 1 μm at 35kh (600 °C). Their occurrence eventually leads to a degradation of the mechanical properties, which will be described in subsequent works.

The formation of V-containing Z-phase in 9–12% Cr steels was widely investigated in the past [20,27–29]. The increase in Z-phase was found to be associated with degradation of mechanical properties, e.g., dramatic loss of creep strength [27]. It was suggested that the large Z-phase grows at the expense of the small highly dispersed MX precipitates, that have a larger strengthening effect than large Z-phase particles.

Laves phase particles were detected at 500 °C and 550 °C. At 500 °C, the Laves phase was detected only in the sample annealed for 108kh, whereas at 550 °C they were detected starting from 21kh. Since some particles reach a size of up to 250 nm after 21kh, their formation starts probably already at few thousand hours. After annealing times up to 75kh, the particles form mainly at the grain boundaries, while at longer times their formation in the grain interior could be often observed (Fig. 7c). The fraction of Laves phase particles with a size < 100 nm is relatively small at all annealing times (Fig. 8).

At 500 °C, the Laves phase forms and grows in a different way than at 550 °C. The main fraction of Laves phase particles observed at 500 °C consist of small < 100 nm particles that are mainly located on the $M_{23}C_6$ precipitates, whereas at 550 °C, the particles have a more globular shape and are mainly located at the grain boundaries. The fraction of small particles (<200 nm) compared to the large (>200 nm) Laves phase particles can be estimated to 25:1. This result indicates that $M_{23}C_6$ precipitates, which can have up to 10 Laves phase particles, served as nucleation sites for its formation (Fig. 6). This results in the highly dispersed formation of Laves phase particles.

In several cases, it can be observed that narrow Laves phase particles form along the grain boundary or between two $M_{23}C_6$ precipitates. Such structure were often observed in EUROFER97 annealed at 500 °C for 108kh, whereas at 550 °C they are present only at 21kh. Such narrow particles demonstrate an initial stage of Laves phase formation, in which W diffusion along the grain boundary plays an important role [30]. In some cases, however, was observed that such narrow Laves phase nuclei have formed inside an $M_{23}C_6$ particle (Fig. 14). The concentration profile clearly shows a decrease of Cr and an increase of W intensity, which supports the fact that the Laves phase particles are located inside $M_{23}C_6$ precipitate.

Conventionally, Laves phase is often considered to influence the microstructure and mechanical properties of those steels [11,12]. It forms during service exposure, and during the growth phase it becomes larger than most other particles, but the coarsening rate is slower than $M_{23}C_6$ [10]. Similar studies with times up to 100kh were performed on the F82H alloy, which falls into the same class of reduced activation steels as EUROFER97 alloy [16]. The steel was analyzed by XDR analysis on the replica, which provides information on the occurrence of different phases but not on the size of the precipitates. Although the F82H alloy has similar V and N content, the formation of a Z-phase was not reported. At the same time, the Laves phase was found to form in the range from 550 °C to 650 °C, which is higher than in our study. At 650 °C the presence of Laves phase was detected already after 3kh annealing. The reason for this difference could be the higher W content (2%) in the F82H steel, while EUROFER97 contains only 1% W. In generally the time temperature formation diagram of these both alloys are very similar.

The formation of Laves phase at 550 °C was reported for CLAM steel [21]. This correlates with our results as the CLAM steel is more similar to EUROFER97 than F82H steel. It can be concluded that a higher or lower W content might play an important role in the formation of the Laves phase. However, despite the extensive research on long-term aging of CLAM steels, the formation of a Z-phase has not been reported.

5. Conclusions

The work presents microscopical analysis of EUROFER97 after annealing in the temperature range from 450 °C to 650 °C and times up to 122kh. The study focuses on analysis of the size and composition of precipitates present in untreated material, e.g. MX and $M_{23}C_6$, as well as on identification and analysis of new precipitates consisting of modified Z and Laves phases. The precipitates were analyzed by EDX, EELS methods and additionally verified using high resolution TEM structural analysis. The results of the present study can be summarized as follows:

- Time-temperature diagram showing the evolution of precipitates in EUROFER97 was plotted in range from 450 °C to 650 °C up to an annealing time of 122 kh. The diagram shows the annealing conditions under which the microstructure remains stable, as well as the conditions under which the formation of Laves and Z-phase can be expected.
- The formation of a modified Z-phase (CrVN) was detected at 550 °C and 600 °C. The size of the Z-phase particles can reach up to 1 μm. At

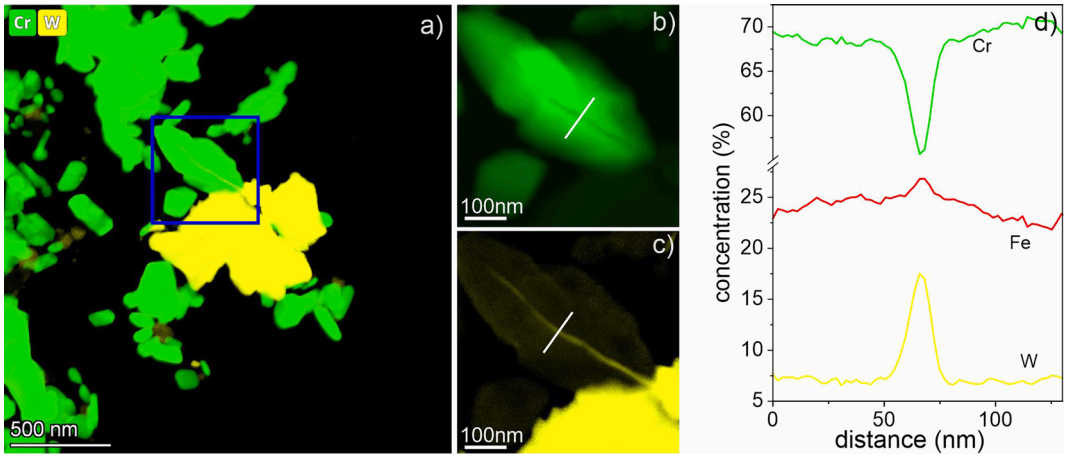

Fig. 14. TEM observation of a narrow Laves phase particle inside $M_{23}C_6$ precipitate (a). Parts (b) and (c) show the Cr and W maps of the area marked by a square, and part (d) presents Cr, Fe and W concentration profiles along the white line.

600 °C, the formation of Z-phase was observed after only a few thousand hours.
- Formation of intermetallic WFe_2 Laves phase was observed at 500 °C and 550 °C. At annealing times of>120kh, the size of Laves phase particles can reach up to 1 μm.
- The temperature-induced alterations to the existing precipitates can be summarized as follows:
  - The size of $M_{23}C_6$ precipitates and MX precipitates increases significantly at 650 °C. At lower temperatures the size of $M_{23}C_6$ particle moderately increases (600 °C) or even slightly decreases (<600 °C). The size of MX precipitates decreases slightly at lower annealing temperatures.
  - The composition of the precipitates changes only slightly. Cr content in the $M_{23}C_6$ precipitates increases with increasing annealing temperature from 67% to 75%. The V content in (Ta,V)C and (V,Ta)N particles increases slightly with annealing at 650 °C, while their composition does not show significant changes at lower temperatures.

CRediT authorship contribution statement

M. Klimenkov: Conceptualization, Investigation, Methodology, Formal analysis, Writing – original draft. **U. Jäntsch:** Resources, Investigation, Writing – review & editing. **M. Rieth:** Supervision, Project administration, Writing – review & editing. **A. Möslang:** Project administration, Writing – review & editing.

Declaration of Competing Interest

The authors declare that they have no known competing financial interests or personal relationships that could have appeared to influence the work reported in this paper.

Data availability

Data will be made available on request.

References

[1] C. Linsmeier, M. Rieth, J. Aktaa, T. Chikada, A. Hoffmann, J. Hoffmann, A. Houben, H. Kurishita, X. Jin, M. Li, A. Litnovsky, S. Matsuo, A. von Müller, V. Nikolic, T. Palacios, R. Pippan, D. Qu, J. Reiser, J. Riesch, T. Shikama, R. Stieglitz, T. Weber, S. Wurster, J.-H. You, Z. Zhou, Development of advanced high heat flux and plasma-facing materials, Nucl. Fusion 57 (2017) 92007, https://doi.org/10.1088/1741-4326/aa6f71.

[2] G. Pintsuk, G. Aiello, S.L. Dudarev, M. Gorley, J. Henry, M. Richou, M. Rieth, D. Terentyev, R. Vila, Materials for in-vessel components, Fusion Engineering and Design 174 (2022), 112994, https://doi.org/10.1016/j.fusengdes.2021.112994.

[3] R. Lindau, A. Möslang, M. Rieth, M. Klimiankou, E. Materna-Morris, A. Alamo, A.-A.-F. Tavassoli, C. Cayron, A.-M. Lancha, P. Fernandez, N. Baluc, R. Schäublin, E. Diegele, G. Filacchioni, J.W. Rensman, B. Schaaf, E. Lucon, W. Dietz, Present development status of EUROFER and ODS-EUROFER for application in blanket concepts, Fusion Engineering and Design 75–79 (2005) 989–996, https://doi.org/10.1016/j.fusengdes.2005.06.186.

[4] R. Lindau, A. Möslang, M. Schirra, Thermal and mechanical behaviour of the reduced-activation-ferritic-martensitic steel EUROFER, Fusion Engineering and Design 61–62 (2002) 659–664, https://doi.org/10.1016/S0920-3796(02)00178-3.

[5] K. Sawada, H. Kushima, K. Kimura, Z-phase Formation during Creep and Aging in 9–12% Cr Heat Resistant Steels, ISIJ Int. 46 (2006) 769–775, https://doi.org/10.2355/isijinternational.46.769.

[6] H. Wang, A. Kostka, W.E. Goosen, G. Eggeler, J.E. Westraadt, TEM replica analysis of particle phases in a tempered martensite ferritic Cr steel after long term creep, Materials Characterization 181 (2021), 111396, https://doi.org/10.1016/j.matchar.2021.111396.

[7] M. Klimenkov, R. Lindau, E. Materna-Morris, A. Möslang, TEM characterization of precipitates in EUROFER 97, Progress in Nuclear Energy 57 (2012) 8–13, https://doi.org/10.1016/j.pnucene.2011.10.006.

[8] P. Fernández, A. Lancha, J. Lapeña, M. Serrano, M. Hernández-Mayoral, Metallurgical properties of reduced activation martensitic steel Eurofer'97 in the as-received condition and after thermal ageing, Journal of Nuclear Materials 307–311 (2002) 495–499, https://doi.org/10.1016/S0022-3115(02)01013-9.

[9] T. Hirose, K. Shiba, T. Sawai, S. Jitsukawa, M. Akiba, Effects of heat treatment process for blanket fabrication on mechanical properties of F82H, Journal of Nuclear Materials 329–333 (2004) 324–327, https://doi.org/10.1016/j.jnucmat.2004.04.047.

[10] L. Schäfer, M. Schirra, K. Ehrlich, Mechanical properties of low activating martensitic 8–10% CrWVTa steels of type OPTIFER, Journal of Nuclear Materials 233–237 (1996) 264–269, https://doi.org/10.1016/0022-3115(95)00183-2.

[11] G. Stornelli, A. Di Schino, S. Mancini, R. Montanari, C. Testani, A. Varone, Grain Refinement and Improved Mechanical Properties of EUROFER97 by Thermo-Mechanical Treatments, Applied Sciences 11 (2021) 10598, https://doi.org/10.3390/app112210598.

[12] X. Hu, L. Huang, W. Yan, W. Wang, W. Sha, Y. Shan, K. Yang, Evolution of microstructure and changes of mechanical properties of CLAM steel after long-term aging, Materials Science and Engineering: A 586 (2013) 253–258, https://doi.org/10.1016/j.msea.2013.08.025.

[13] Q. Min, Q. Guo-xing, C. Ming-chong, C. Du Qing, W.-Y. Lei, Microstructure Stability and Mechanical Properties of Reduced Activated Ferritic Martensitic Steel during Thermal Aging at 550 °C for 5000 h, J. of Materi Eng and Perform (2022), https://doi.org/10.1007/s11665-022-07498-6.

[14] V.B. Oliveira, H. Sandim, D. Raabe, Abnormal grain growth in Eurofer-97 steel in the ferrite phase field, Journal of Nuclear Materials 485 (2017) 23–38, https://doi.org/10.1016/j.jnucmat.2016.12.019.

[15] F. ABe, Effect of fine precipitation and subsequent coarsening of Fe2W laves phase on the creep deformation behavior of tempered martensitic 9Cr-W steels, Metall Mater Trans A 36 (2005) 321–332, https://doi.org/10.1007/s11661-005-0305-y.

[16] K. Shiba, H. Tanigawa, T. Hirose, H. Sakasegawa, S. Jitsukawa, Long-term properties of reduced activation ferritic/martensitic steels for fusion reactor blanket system, Fusion Engineering and Design 86 (2011) 2895–2899, https://doi.org/10.1016/j.fusengdes.2011.06.005.

[17] L. Cui, Y. Dai, S.S. Gerstl, M.A. Pounchon, APT characterization of irradiation effects on MX phase in reduced-activation ferritic/martensitic steels, Journal of Nuclear Materials 573 (2023), 154121, https://doi.org/10.1016/j.jnucmat.2022.154121.

[18] H.K. Danielsen, J. Hald, Tantalum-containing Z-phase in 12%Cr martensitic steels, Scripta Materialia 60 (2009) 811–813, https://doi.org/10.1016/j.scriptamat.2009.01.025.

[19] H.K. Danielsen, J. Hald, F.B. Grumsen, M.A.J. Somers, On the crystal structure ofZ-phase Cr(V, Nb)N, Metall Mater Trans A 37 (2006) 2633–2640, https://doi.org/10.1007/BF02586098.

[20] F. Liu, M. Rashidi, L. Johansson, J. Hald, H.-O. Andrén, A new 12% chromium steel strengthened by Z-phase precipitates, Scripta Materialia 113 (2016) 93–96, https://doi.org/10.1016/j.scriptamat.2015.10.030.

[21] L. Yang, F. Zhao, W. Ding, Laves Phase Evolution in China Low-Activation Martensitic (CLAM) Steel during Long-Term Aging at 550 °C, Materials (Basel) 13 (1) (2019) 154, https://doi.org/10.3390/ma13010154.

[22] M. Roldán, E. Leon-Gutierrez, P. Fernández, A. Gómez-Herrero, Deformation behaviour and microstructural evolution of EUROFER97-2 under low cycle fatigue conditions, Materials Characterization 158 (2019), 109943, https://doi.org/10.1016/j.matchar.2019.109943.

[23] M. Rieth, M. Schirra, A. Falkenstein, P. Graf, S. Heger, H. Kempe, R. Lindau, H. Zimmermann, EUROFER 97. Tensile, charpy, creep and structural tests, Karlsruhe, 2003.

[24] D. Zagorac, H. Müller, S. Ruehl, J. Zagorac, S. Rehme, Recent developments in the Inorganic Crystal Structure Database: theoretical crystal structure data and related features, J. Appl. Crystallogr. 52 (2019) 918–925, https://doi.org/10.1107/S160057671900997X.

[25] Y. Zhang, G. Li, F. Yuan, F. Han, M. Ali, W. Guo, J. Ren, C. Liu, H. Gu, G. Yuan, The formation mechanism of stacking faults in ZrFe2 Laves phase in Zircaloy-4 alloy, J Mater Sci 56 (2021) 11164–11173, https://doi.org/10.1007/s10853-021-05984-1.

[26] A. Aghajani, C. Somsen, G. Eggeler, On the effect of long-term creep on the microstructure of a 12% chromium tempered martensite ferritic steel, Acta Materialia 57 (2009) 5093–5106, https://doi.org/10.1016/j.actamat.2009.07.010.

[27] A. Strang, V. Vodarek, Z phase formation in martensitic 12CrMoVNb steel, Materials Science and Technology 12 (1996) 552–556, https://doi.org/10.1179/mst.1996.12.7.552.

[28] L. Cipolla, H.K. Danielsen, D. Venditti, P.E. Di Nunzio, J. Hald, M.A. Somers, Conversion of MX nitrides to Z-phase in a martensitic 12% Cr steel, Acta Materialia 58 (2010) 669–679, https://doi.org/10.1016/j.actamat.2009.09.045.

[29] H.K. Danielsen, J. Hald, Behaviour of Z phase in 9–12%Cr steels, Energy Materials 1 (2006) 49–57, https://doi.org/10.1179/174892306X99732.

[30] M.I. Isik, A. Kostka, G. Eggeler, On the nucleation of Laves phase particles during high-temperature exposure and creep of tempered martensite ferritic steels, Acta Materialia 81 (2014) 230–240, https://doi.org/10.1016/j.actamat.2014.08.008.